Ⓔ

A Shallow Earthquake Swarm Close to Hydrocarbon Activities: Discriminating between Natural and Induced Causes for the 2018–2019 Surrey, United Kingdom, Earthquake Sequence

by Stephen P. Hicks, James Verdon, Brian Baptie, Richard Luckett, Zoë K. Mildon, and Thomas Gernon

ABSTRACT

Earthquakes induced by subsurface industrial activities are a globally emotive issue, with a growing catalog of induced earthquake sequences. However, attempts at discriminating between natural and induced causes, particularly for anomalously shallow seismicity, can be challenging. An earthquake swarm during 2018–2019 in southeast England with a maximum magnitude of M_L 3.2 received great public and media attention because of its proximity to operating oilfields. It is therefore vital and timely to provide a detailed characterization of the earthquake sequence at present, and to decide based on current evidence, whether the earthquakes were likely natural or induced. We detected 168 low-magnitude earthquakes and computed detailed source parameters of these events. Most earthquakes occurred at a shallow depth of 2.3 km, >1 km deeper than the geological formations targeted by the oilfields, and laterally >3 km away from the drill sites. We combine the east–west-trending cluster of the seismicity with 2D seismic reflection profiles to find the causative fault system for the earthquakes. A *b*-value close to unity and strike-slip faulting mechanisms are consistent with tectonic reactivation along a pre-existing fault. Overall, we find no indicators in the earthquake parameters that would strongly suggest an induced source. Nor do we find any clear trends between seismicity and drilling activities based on operational logs provided by the operators. Injected volumes are near zero and monthly production amounts are many orders of magnitude smaller than other reported cases of extraction-induced seismicity. On balance, and based on the available evidence, we find it currently unlikely that nearby industrial activities induced the seismic swarm. Most likely, the Surrey earthquakes offer a uniquely detailed insight into shallow seismicity within sedimentary basins. Nevertheless, self-reporting of injection and production times and volumes by operators, and the lack of easily and publicly available oilfield operational data continues to be a point of concern for local residents.

Supplemental Content: Notes on velocity model and relocation, magnitude estimation, waveform moment tensor inversion, stress-drop estimates from displacement spectra, static Coulomb stress modeling, fault mapping from 2D seismic profiles, and moment tensor dip uncertainty, tables of layered velocity model, summary of hypocenter parameters relocated using NonLinLoc, and static stress transferred to the epicentres of the $M_w > 2$ earthquakes in the sequence from all prior $M_w > 2$ earthquakes, and figures showing 1D velocity model, hypoDD relocations, spectral fits, scatter plot showing local magnitude versus hour of day for all detected events, scaling between M_L and M_w, estimated stress drops, correlation between magnitude and depth, and static stress changes.

INTRODUCTION

In recent years, seismicity induced and triggered by industry has become a topic of great scientific and public interest around the world. Seismic events near industrial facilities alarm local communities and large events can cause financial losses to residents, yet discriminating between anthropogenic and natural seismicity is not a trivial task (Grigoli *et al.*, 2017).

These issues emerged during a sequence of small, yet shallow earthquakes that began on 1 April 2018, a few kilometers from the villages of Newdigate and Charlwood in Surrey, United Kingdom (Figs. 1 and 2), and within 10 km of two

doi: 10.1785/0220190125

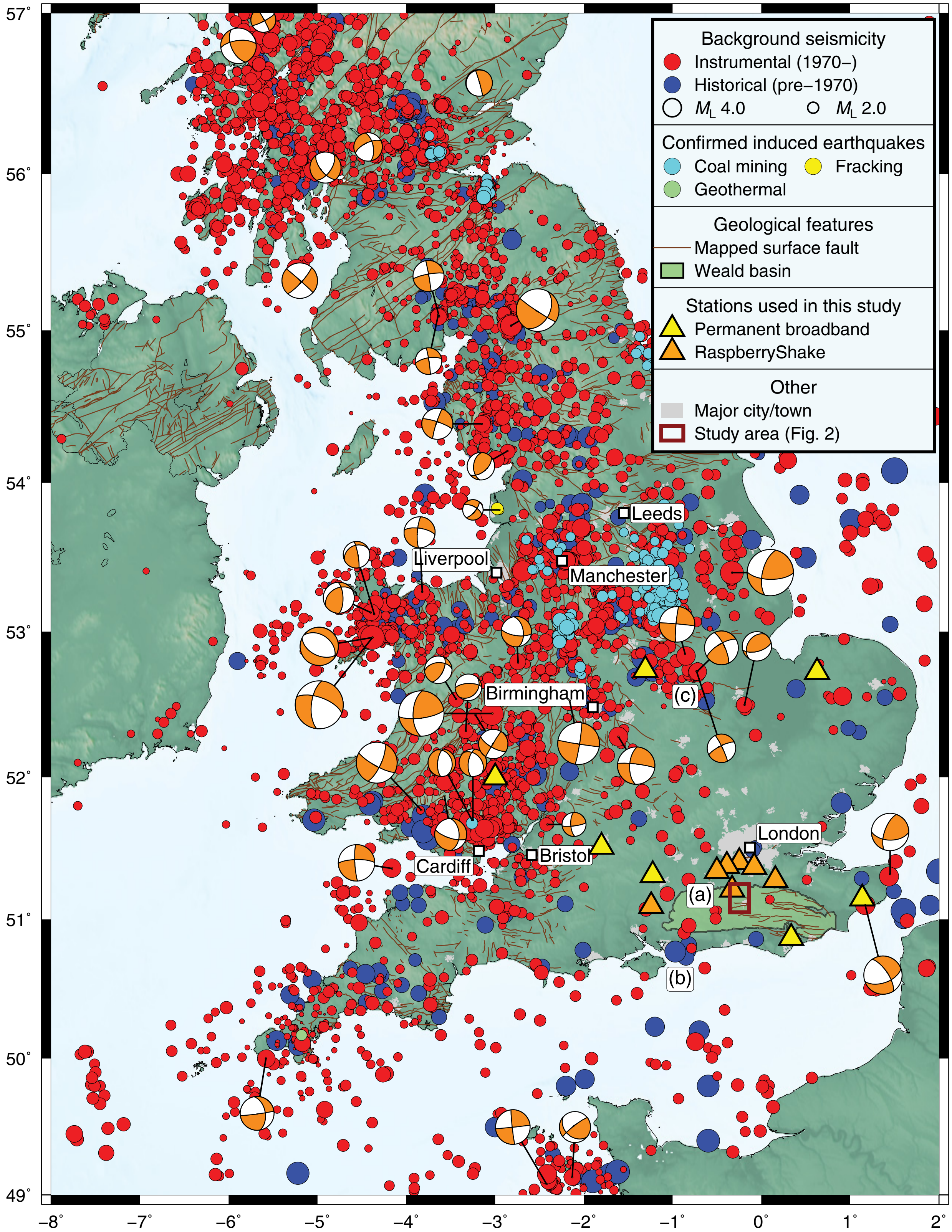

▲ **Figure 1.** Regional context showing the study area (brown rectangle), together with instrumental and historical seismicity context of England and Wales from the British Geological Survey (BGS) catalog. Induced earthquakes are from Wilson *et al.* (2015). Regional seismic stations used in this study are shown. Mapped surface fault traces come from BGS (2019). Past earthquake focal mechanisms (orange focal mechanism plots) come from Baptie (2010) and from BGS annual earthquake bulletin reports. Labels (a) and (b) refer to the 2005 Billingshurst and 1811–1834 Chichester sequence, respectively, which are discussed in the Regional Seismological, Geological, and Industrial Context section. The color version of this figure is available only in the electronic edition.

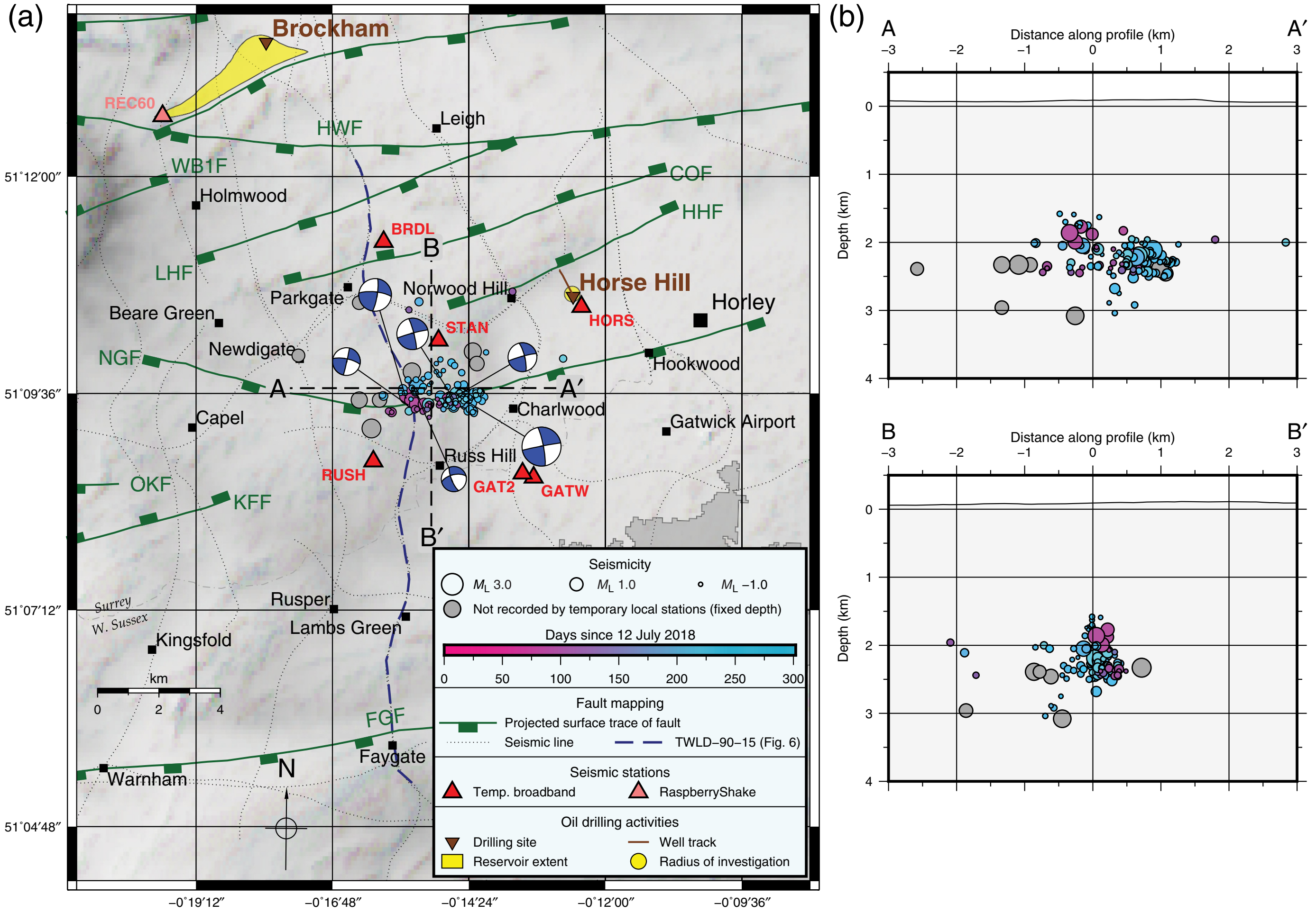

▲ **Figure 2.** (a) Map of the study area showing relocated earthquakes of the 2018–2019 Newdigate sequence, focal mechanisms, mapped faults, local seismic stations, 2D seismic lines (Ⓔ Note S6), and the locations of oilfield activities. Only high-quality earthquake hypocenters are plotted with a maximum azimuthal gap of less than 200°. Earthquake locations are colored to show their evolution through time. Dark gray circles indicate earthquakes that occurred before the installation of the temporary local seismic network, and therefore have uncertain locations, with fixed depths. 2D seismic profile TWLD 90-15 is shown in Figure 6. (b) North–south and west–east cross sections of seismicity with event hypocenters. The cross-section locations are labeled on the map. BHF, Box Hill fault; BRF, Brockham fault; BUF, Buckland fault; COF, Collendean fault; FGF, Faygate fault; HHF, Horse Hill fault; HWF, Holmwood fault; KFF, Kingsfold fault; LHF, Leigh fault; NGF, Newdigate fault; OKF, Ockley fault; WB1F, Whiteberry-1 fault; WCF, Westcott fault. The color version of this figure is available only in the electronic edition.

actively operating oilfield discovery and production sites at Brockham and Horse Hill. The British Geological Survey (BGS) detected 34 small earthquakes between April 2018 and May 2019. Nearby people in large settlements, such as Crawley, Dorking, and Gatwick Airport, felt many of the earthquakes. Residents described shaking from the largest earthquake (M_L 3.2) corresponding to a maximum intensity of 5 (strong shaking) on the European Macroseismic Scale (EMS; Grünthal, 1998; British Geological Survey [BGS], 2019). Southeast and southern England, which encompasses the Weald and Wessex basins, has a relatively low background earthquake activity rate in comparison to other parts of Britain (Musson and Sargeant, 2007); few similar sequences have been recorded in the past (Fig. 1). This lack of past precedence together with the proximity to nearby hydrocarbon activities meant that the seismic sequence attracted widespread public and media interest (e.g., Webster, 2018).

Research has shown that many forms of industrial activities can induce seismicity. These include: conventional hydrocarbon production (Segall, 1989), stimulating geothermal reservoirs (Häring *et al.*, 2008), hydraulic fracturing (Clarke *et al.*, 2014), CO2 storage (Kaven *et al.*, 2015), mining (e.g., Wilson *et al.*, 2015), and wastewater injection (Keranen *et al.*, 2014). Induced seismicity caused by fluid injection has been observed to occur both within crystalline basement (Verdon, 2014), and the shallower sedimentary formations being targeted by these operations (Eaton *et al.*, 2018). The poroelastic response of shallow sedimentary rocks to large changes in fluid pressure over great distances is poorly understood (Goebel and Brodsky, 2018).

Conversely, anomalous seismic swarms occurring at shallow depth can have natural causes (e.g., Bent *et al.*, 2017). Natural earthquakes close to industrial sites heighten public concern and can cause financial loss to operating companies if misattributed as induced; an example being the 2015 M_w 6.1 Emilia, Italy, earthquake (Dahm *et al.*, 2015; Grigoli *et al.*, 2017). Overall, the mechanisms and occurrence statistics of very shallow earthquakes are poorly constrained.

Criteria to discriminate induced versus natural seismicity include answering qualitative questions (Davis and Frohlich, 1993; Verdon *et al.*, 2019), and more quantitative analyses such as earthquake source studies, numerical modeling, and statistical tests (Grigoli *et al.*, 2017).

The United Kingdom is an area where induced earthquakes are a highly contentious issue. The background seismicity rate is low, with the regional state of stress dominated by northwest–southeast compression from the Mid-Atlantic Ridge and the Mediterranean (Baptie, 2010). Most earthquakes occur in the north and west of mainland Britain (Fig. 1). Anthropogenic earthquakes in the U.K. account for ~20% of all earthquakes in the instrumental catalog (Wilson *et al.*, 2015). The greatest contributor has been coal mining (Kusznir *et al.*, 1980; Verdon *et al.*, 2018) in central–northern England, South Wales, and Scotland (Fig. 1). The maximum observed magnitude from coal mining induced seismicity is M_L 3.1 (Redmayne, 1988; Bishop *et al.*, 1993; Wilson *et al.*, 2015). For geothermal induced seismicity, over 11,000 microseismic events were detected during the Hot Dry Rock project in southwest England between 1982 and 1987 (Pine and Batchelor, 2001). The largest event had a magnitude of M_L 2.0. Although no operators in the Weald basin in southeast England conducted, nor applied to do hydraulic fracturing, the U.K.'s Traffic Light Scheme for hydraulic fracturing-induced seismicity received extensive media attention. 31 events in the Surrey swarm had magnitudes that exceed the current M_L 0.5 red light threshold.

For hydrocarbon extraction, the largest induced event to occur in the United Kingdom was the 2001 M_w 4.3 Ekofisk, North Sea earthquake with water injection causing shallow slip in the overburden at <3 km depth (Ottemöller *et al.*, 2005). In 2011, the first U.K. onshore hydraulic fracturing of shale took place near Blackpool in northern England. Injection triggered an M_L 2.3 earthquake, ~1.8 km from the Preese Hall-1 well, at 3.6 km depth (Clarke *et al.*, 2014). Hydraulic fracturing and induced microseismicity resumed nearby in 2018 at Preston New Road, drawing public attention once again to anthropogenic earthquakes (Clarke *et al.*, 2019). Most past induced earthquakes in the United Kingdom are small ($M_L < 3.1$) and occur at shallow depth (<3 km). Therefore, accurately characterizing earthquake sources and understanding the causes of such weak near-surface seismicity is challenging in areas with sparse seismic station coverage. This was an issue for the 2018–2019 Surrey seismic sequence, for which the nearest permanent station of the BGS national seismic network lies on the southern coast of England, over 50 km away (Fig. 1). This network sparsity made it difficult to initially constrain depth and faulting mechanisms, which can help to discriminate between natural and induced causes (Frohlich *et al.*, 2016). The strong macroseismic intensity observations supported early shallow depth estimates (initially fixed to 5.0 km), raising further suspicions over possible induced seismicity (Verdon *et al.*, 2019).

After the 10th recorded earthquake, we installed a network of five temporary broadband seismometer stations in the epicentral region (Fig. 2). Given the large interest in these earthquakes, here we analyze available seismic data to make a coherent seismological analysis of the 2018–2019 Surrey earthquake sequence up to July 2019. We interpret these events in terms of the regional geological structure of the Weald basin. We compare the spatiotemporal evolution of the seismicity with reported activities associated to oilfield development and production at the nearby Horse Hill and Brockham sites to understand its cause.

REGIONAL SEISMOLOGICAL, GEOLOGICAL, AND INDUSTRIAL CONTEXT

Southern and southeast England is one of the least seismically active areas in the United Kingdom (Fig. 1). The largest instrumentally recorded event in the region was the M_L 4.3 earthquake in Folkestone in 2009. The depth of this event, constrained by both teleseismic observations and regional waveform modeling, was at 5 ± 2 km (Ottemöller *et al.*, 2009). There is also considerable evidence for damaging earthquakes in the Dover Straits over the last 1000 yr, for example, an estimated M_L 5.8 earthquake in 1580 (García-Moreno *et al.*, 2015). There are only a few recorded earthquakes within the Weald basin itself. In 2005, there were three small earthquakes near Billingshurst (Fig. 1, label a), ~24–34 km southwest of the Newdigate sequence. The largest earthquake of the Billingshurst sequence had a magnitude of M_L 2.1 and a shallow depth—likely less than 5–10 km (Baptie and Luckett, 2018). Historical catalogs provide evidence for past earthquakes in the Weald region over the last 500 yr. For example, Musson (2008) found reports of an earthquake on 5 May 1551. Although the limited macroseismic data mean that a location and magnitude cannot be determined, the reports suggest that it was strongly felt with an intensity of 5 EMS in Dorking, ~8 km from the 2018–2019 earthquake swarm. Further afield, there were six earthquakes near Chichester on the south coast (Fig. 1, label b) in the 1800s with estimated magnitudes of M_L 2.9–3.4 (Musson, 1994). Such earthquake sequences or swarms are relatively common in Great Britain. Examples include Comrie, 1788–1801 and 1839–1846 (Musson, 1993); Kintail, 1974 (Assumpção, 1981); Manchester, 2002–2003 (Baptie and Ottemoeller, 2003); and Aberfoyle, 2003 (Ottemöller and Thomas, 2007). More recently, in 2014–2015 there was a sequence of earthquakes near Oakham (Fig. 1, label c) in the East Midlands of England. The three largest events had magnitudes of M_L 3.2, 3.5, and 3.8, with depths of less than 5 km. None of the above sequences were linked to anthropogenic causes, although the Manchester sequence occurred in a sedimentary basin where coal had been mined in the past.

The epicentral area of the Newdigate sequence in the Weald basin comprises uplifted sedimentary rocks spanning southeast England, the eastern English Channel and northern France (Fig. 1). A wealth of 2D seismic data from the UK Onshore Geophysical Library (UK Onshore Geophysical Library [UKOGL], 2019) allows for a robust characterization of basin structure. The top Palaeozoic basement beneath the center of the Weald lies at 2500–3000 m depth (Butler and Pullan, 1990). An interpreted regional seismic profile that runs ~20 km west of Newdigate shows sedimentary fill extending to depths of >3000 m in the basin center (UKOGL, 2019).

Oil drilling in the Weald targeted Jurassic rocks, including conventional reservoirs such as the Portland sandstone and the Great Oolite, and lower permeability formations such as the Kimmeridge Clay (Andrews, 2014). The Mesozoic basin sediments sit unconformably on Devonian-to-Lower Carboniferous Palaeozoic sedimentary rocks, which have been deformed, but not metamorphosed, by the Variscan orogeny (Butler and Pullan, 1990). Boreholes rarely penetrated pre-Variscan units, and therefore they are less well studied.

The key structural features of the Weald basin were originally formed during the Variscan (Hansen *et al.*, 2002), generating east–west-trending thrust faults. These were reactivated as extensional faults during the Permian as postorogenic collapse, forming the basin. We find large extensional structures running through the Triassic and Jurassic sedimentary rocks, rooted in the underlying basement and preserving the original east–west trend, with most dipping to the south.

Angus Energy Plc. operates the Brockham oilfield, ~8 km away from the earthquakes (Fig. 2). Brockham produced relatively small volumes from the Portland sandstone, with ~60, 000 m^3 gross water and oil since 2002. Formation water produced is reinjected back into the reservoir. Overall, net output is greater than net injection. Production volumes since 2002 have been in decline, with several pauses in operations over the years. The most recent pause in operations occurred between February 2016 and March 2018. In 2017–2018, development work from a sidetrack well targeted the deeper Kimmeridge Clay formation.

Known colloquially as the Gatwick Gusher, the Horse Hill-1 (HH-1) discovery well lies ~3 km away from the earthquake swarm (Fig. 2). Operated by Horse Hill Developments Limited (HHDL), drilling of HH-1 was completed in October 2014. HHDL first flow-tested the Portland sandstone at ~600 m depth in March 2016, and limestone bands within the Kimmeridge Clay formation at ~800 m depth in February 2016. To date, ~7000 m^3 of oil has been produced at HH-1 since July 2018. According to the operator, no water is currently being produced at the well, and no fluids are typically injected into the reservoir.

DATA AND METHODS

Seismic waveforms for the first events in the sequence (April–July 2018) were recorded on the BGS national broadband seismic network (Fig. 1). In southeast England, there are several RaspberryShake (RS) stations with geophone sensors (Anthony *et al.*, 2018), which improve the recording coverage of the earthquakes (Fig. 1). The closest RS station (AM.REC60) lies ~6 km from the epicentral region of the swarm (Fig. 2). After the first nine events, we installed a network of five temporary stations in the area (Fig. 2) comprising Güralp 3ESPC 30 s–100 Hz seismometers, with a sampling rate of 200 Hz. We installed two of these stations (GB.HORS and GB.RUSH) in mid-July and three (GB.GATW, GB.STAN, and GB.BRDL) in early August 2018 (Fig. 3a). We analyzed seismic waveform data up until 3 July 2019 (see Data and Resources).

We derive our 1D seismic velocity model from detailed sonic log information from nearby boreholes (Ⓔ Note S1, Ⓔ Fig. S3, and Ⓔ Table S1 available in the supplemental content to this article). We find that the resulting earthquake locations are relatively insensitive to any deviations from this assumed velocity structure (Ⓔ Note S1). To relocate the earthquakes, we used NonLinLoc (Lomax *et al.*, 2009), which offers robust constraints on location uncertainties compared with traditional single-event location codes. To assess any smaller scale structure in the spatiotemporal evolution of the seismicity, we also computed double-difference relocations (Waldhauser and Ellsworth, 2000) (Ⓔ Note S1). We selected ~19, 000 delay time pairs each for *P*- and *S* waves and ~15, 000 and ~18, 000 cross-correlation times for *P*- and *S* waves, respectively, for the double-difference relocation. We computed magnitudes using the U.K. local magnitude (M_L) scale of Luckett *et al.* (2019), suitable for near-field observations (Ⓔ Note S2).

To detect further low-magnitude seismicity not in the initial BGS catalog, we took two approaches. (1) We used the Lassie software (Heimann, 2016; López-Comino *et al.*, 2018), a stack-and-delay-based coherence detector, to find and locate events using continuous data from the temporary seismic network. Coherency is mapped using a smooth characteristic function calculated from normalized waveform envelopes. From this catalog, we then (2) ran a cross-correlation template-matching algorithm on data from local stations. For this, we used 1.0 s long template waveforms incorporating *P*- and *S* waves from the events in the catalog. We utilized EQcorrscan (Chamberlain *et al.*, 2018) to scan for earthquakes on data filtered at 5–15 Hz. Detections were made when the network-stacked cross-correlation sum exceeded nine times the median absolute deviation. We then manually repicked and relocated positive detections. For nearby RS station AM.REC60, we also scanned continuous waveforms before the first known earthquake, extending back as far as September 2017, when this station was first installed. There were no earlier positive detections; therefore, no significantly larger earthquake ($M_L > 1.5$) likely occurred here before 1 April 2018, so the main sequence probably started then.

To investigate the causal mechanism of the Newdigate earthquakes, we computed moment tensors from waveforms, Gutenberg–Richter *b*-values, stress drops from displacement spectra, and static stress transfer (see Ⓔ Notes S3, S4, and S5).

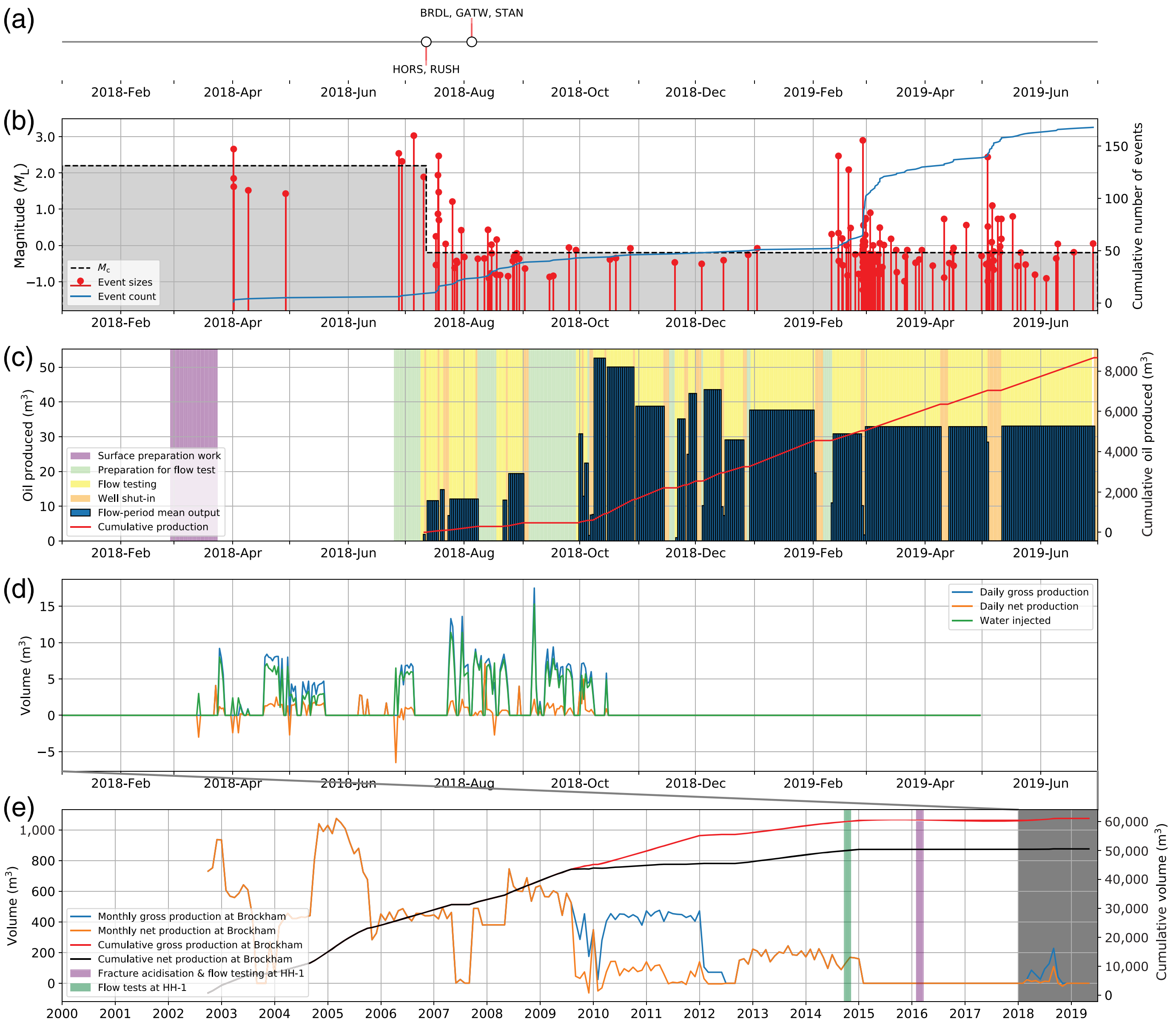

▲ **Figure 3.** Timeline comparing evolution of the Newdigate seismic swarm with nearby oil field activities. (a) Installation dates of the local temporary seismic monitoring network. (b) Detected seismicity, cumulative number of events, and the gray shaded area indicating the approximate completeness magnitude of the catalog over time. (c) Horse Hill-1: operations timeline (shaded boxes; see Ⓔ Table S4) together with flow-period averaged production and cumulative production over time. (d) Daily reservoir production and injection values at Brockham. (e) A long-term view of operations, with the time interval shown in panels above covering the 2018–2019 period delineated by the gray box and connecting lines. The color version of this figure is available only in the electronic edition.

RESULTS

Besides the 34 events recorded in the BGS catalog, we detected a further 135 microearthquakes from 12 July 2018 onward, forming an overall catalog of 168 events (Figs. 2 and 3b; Ⓔ Table S2). Hypocenters for well-constrained events recorded by five temporary monitoring stations have a mean depth of 2.3 km. Most locations have formal epicentral and depth uncertainties of <200 and <500 m, respectively (Ⓔ Fig. S5). These solutions are robust as they vary little when relocated in different velocity models, and they had low root mean square arrival-time residuals (<60 ms). Given the high-waveform similarity between large events (Fig. 4), we fixed the depth of events before 12 August 2018 to 2.3 km (Ⓔ Note S1).

Overall, the best-constrained events illuminate a seismogenic patch ~2.5 km long and extending over 1.3 km in depth (Fig. 2). Most event epicenters in our full catalog appear to cluster along a roughly linear band, trending east–west. A few microseismic events were detected up to 2 km away to the north and east of the main cluster of seismicity. High-precision

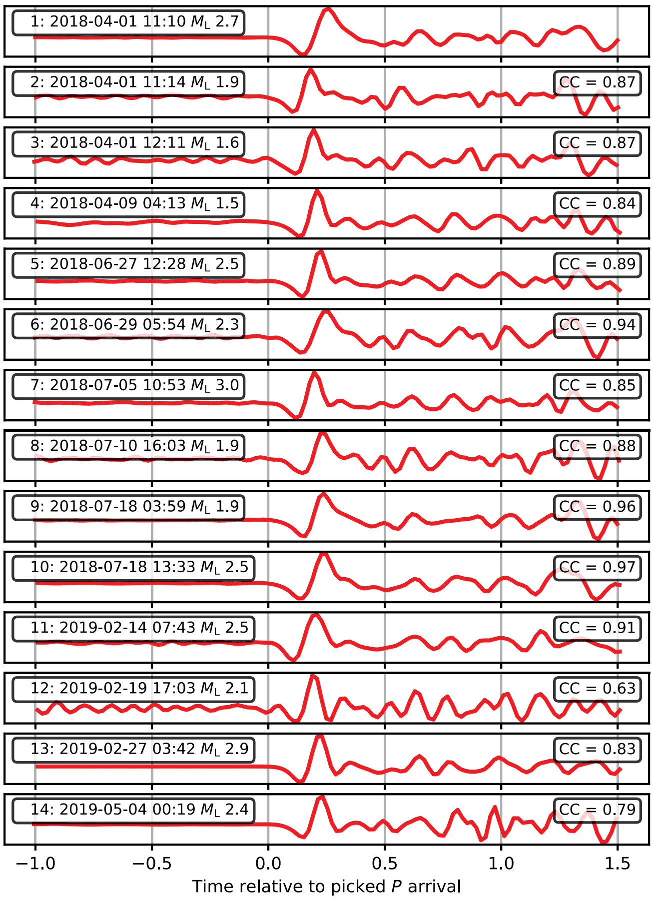

▲ **Figure 4.** Low-pass filtered (10 Hz) vertical-component waveforms recorded at RaspberryShake (RS) station REC60 (~8 km epicentral distance) showing similarity between the largest events ($M_L > 1.5$) of the Newdigate sequence. Waveform cross-correlation (CC) values computed in a window starting 0.02 s and ending 0.70 s after the picked *P*-wave arrival are labeled and are calculated with respect to the first event in the sequence (1). The color version of this figure is available only in the electronic edition.

double-difference relocations of 95 events (mean epicenter error: ~50 m; mean hypocenter depth error: ~60 m) confirm the strong east–west alignment of seismicity (Ⓔ Fig. S6). Although the single-event locations indicate an apparent west-to-east migration in seismicity with time (Fig. 2), we find that this is an artifact due to greater location uncertainties for events that occurred in July to early August 2018 and were only recorded by the first two stations installed of the temporary network. Moreover, the double-difference relocations show no similar migration with time (Ⓔ Fig. S6).

The temporary stations captured six of the larger earthquakes ($M_L \geq 1.9$) in July 2018 and February 2019 (Fig. 3a,b), allowing us to probe rupture mechanisms and depths (see Fig. 5). The best-constrained moment tensor solutions have centroid depths of 2.2 ± 0.2 km, consistent with hypocenters (Ⓔ Fig. S7) and show the same purely strike-slip faulting mechanism. The west–east nodal plane corresponds to the alignment of seismicity (Fig. 2). The double-couple percentage is high (>75%). Analysis of 218 *P*-wave polarities from the wider catalog suggests that most events had this same mechanism, with little variability (Fig. 5c).

In Figure 2, we examine whether this cluster of earthquakes correlates with pre-existing faults identified from 2D seismic profiles (Ⓔ Note S6). Faults within the Mesozoic sediments are relatively easy to find, most of which strike east–west and dip toward the south. We also find north-dipping and east-northeast–west-southwest-trending faults. The Newdigate fault (NGF) is a prominent east–west striking, south-dipping fault system showing a normal sense of offset, which extends across much of the study area. Most epicenters lie along the projected surface trace of the NGF, consistent with the west–east nodal plane of the focal mechanisms, suggesting slip occurred along this fault system (Figs. 2 and 5). We can see this overall relationship more clearly in the double-difference relocations (Ⓔ Fig. S6). The Triassic lowermost basin fill and underlying Palaeozoic rocks appear to be more heavily faulted (Fig. 6). Given the spacing of the 2D seismic lines and the number of fault traces, we have not attempted to map the extent of faults in the basement lower units. However, we can assume that these faults have similar trends and positions as the extensional faults that extend above them. The double-difference locations show that most events in fact occurred within the footwall of the NGF; they likely occurred on a south-dipping fault at greater depth within the lowermost basin fill (Fig. 6).

From fitting displacement spectra of earthquakes in the sequence using an ω^2 model (Brune, 1970; see Ⓔ Fig. S8), we compute mean stress drops of 0.2–11.0 MPa (Ⓔ Fig. S9). From modeled static stress changes resulting from the $M_L > 2$ earthquakes, accounting for the depth and the fault geometry uncertainties, we find that most events with $M_L > 2$ occurred in a region of positive static stress from earlier earthquakes (Ⓔ Fig. S10). For $M_L > 2$ earthquakes, we computed the total accumulated static stress at the hypocenter before each earthquake (Ⓔ Table S3) resolved onto fault geometries consistent with the Newdigate and Horse Hill faults. For nearly all $M_L > 2$ earthquakes, changing the depth and/or strike of the receiver faults within the range of uncertainties can cause positive stress changes. Some studies (e.g., Ziv and Rubin, 2000; Ogata, 2005) speculate that there is no lower threshold—any amount of positive stress change could be enough to trigger subsequent earthquakes. For some earthquakes, however, the epicenters were too close, and therefore the static stress calculated is unreliable due to unmodeled near-field slip complexity (Steacy *et al.*, 2004).

We also assess the frequency–magnitude distribution of the Newdigate seismic sequence in terms of the *b*-value of the Gutenberg–Richter relationship. Previous studies (Staudenmaier *et al.*, 2018) show that the different scaling between M_L and M_w for small earthquakes may cause an artificial bilinear Gutenberg–Richter fit. Therefore, we also used our spectral and moment tensor estimates of M_w to rescale the M_L values. We look at several timeframes for this as the temporary local monitoring network was not in place for the start of the earthquake sequence. We compute magnitude of

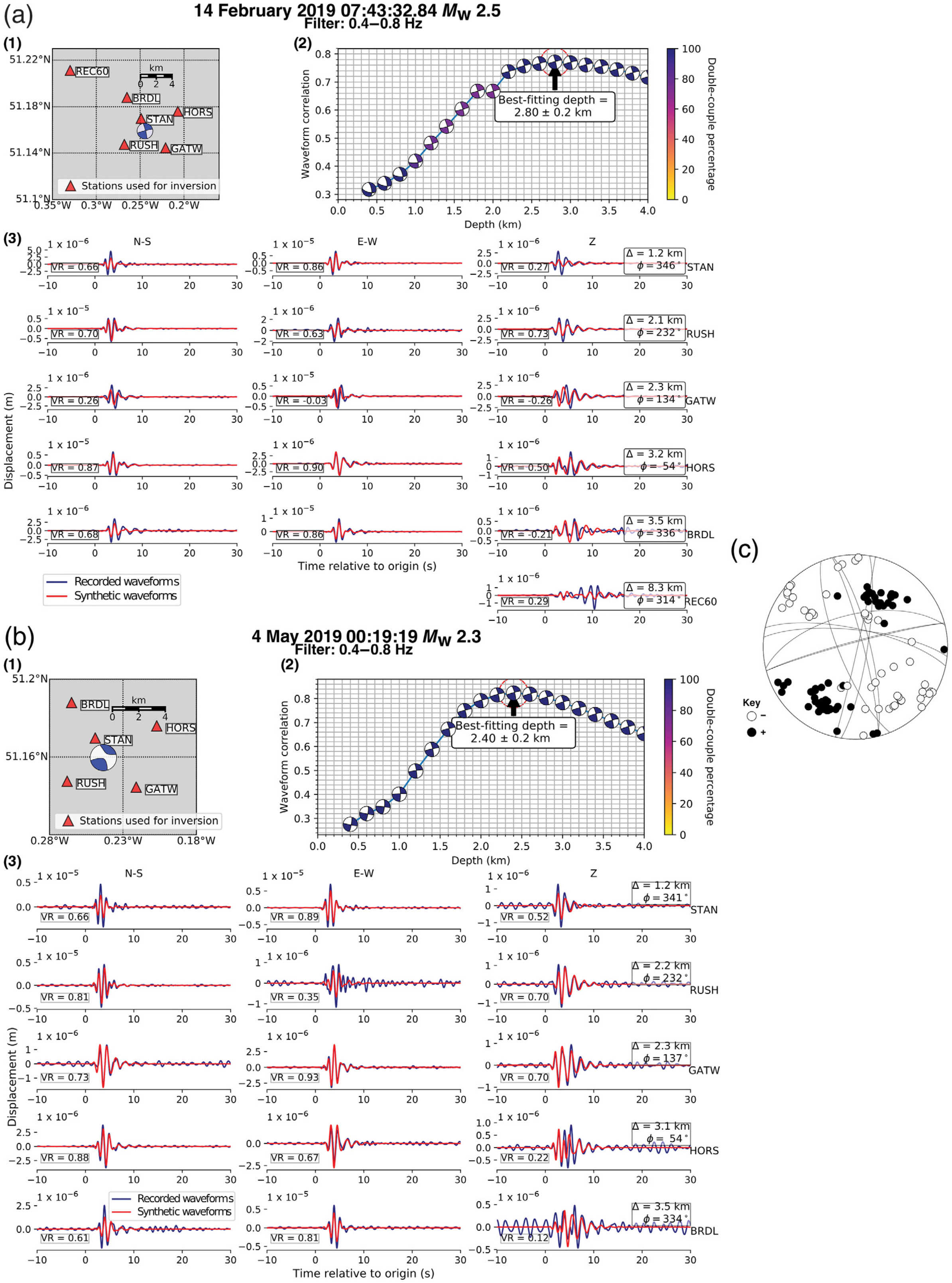

▲ **Figure 5.** (a,b) Representative moment tensor solutions for two earthquakes recorded by all five local stations. (1) Map showing stations and best-fitting focal mechanism, (2) waveform correlation as a function of centroid depth, (3) waveform fits. VR, variance reduction. (c) Observed first-motion *P*-wave polarities from all events in the catalog represent a composite faulting mechanism compared to fault planes from the best-fitting focal mechanisms from moment tensors (a) and (b). The color version of this figure is available only in the electronic edition.

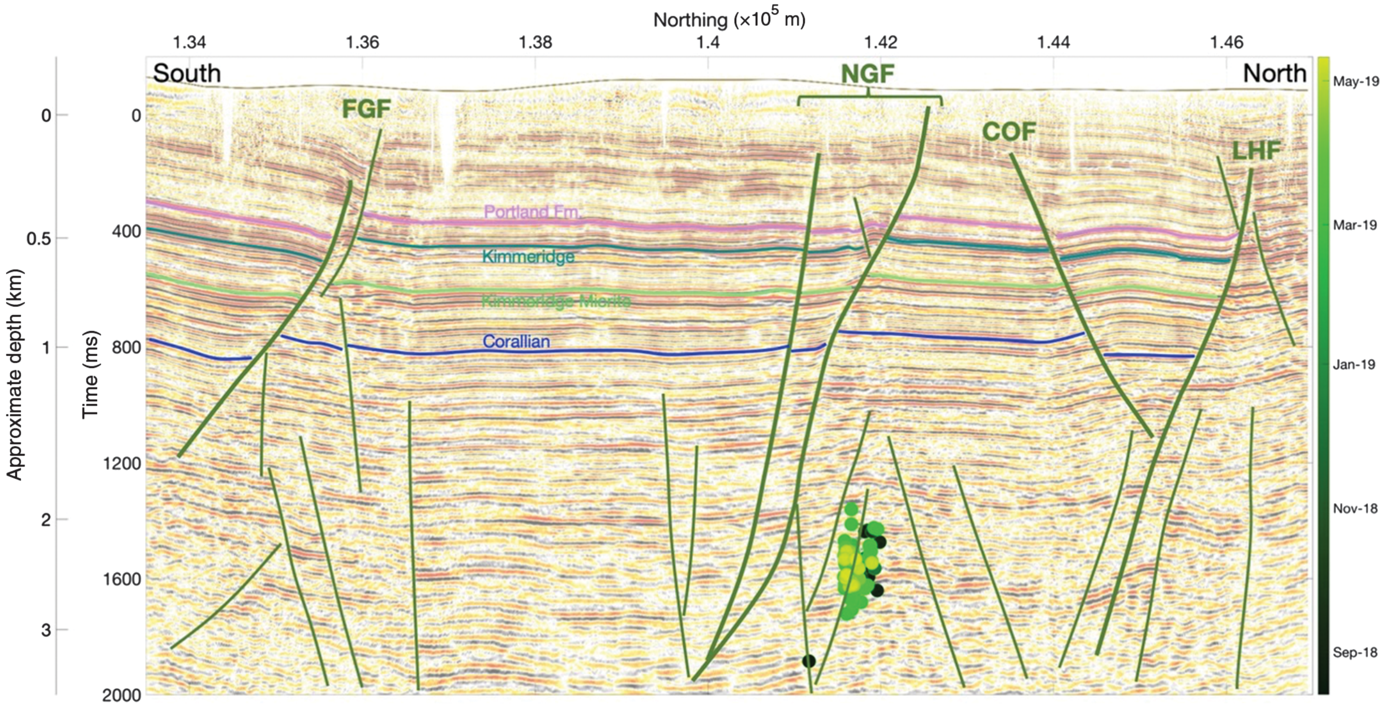

▲ **Figure 6.** 2D seismic section along profile TWLD-90-15 (Fig. 2) showing interpreted faults (green lines), geological formations, together with the projected positions of double-difference 40 relocated earthquakes from this study. The color of each event denotes the time that each event occurred. COF, Collendean fault; FGF, Faygate fault; LHF, Leigh fault; NGF, Newdigate fault. An uninterpreted version of this section is shown in Ⓔ Figure S13. The color version of this figure is available only in the electronic edition.

completeness M_c by minimizing the residual between a power law fit to the data and the observed distribution (Wiemer and Wyss, 2000). First, we consider the entire earthquake sequence starting in April 2018. We find an M_c of ∼2.2, supported by the overall M_c estimate for southeast England (BGS, 2010). For this time period, we find a best-fitting *b*-value of 1.2 (Fig. 7a). For the time when the local temporary monitoring network was operational, we computed a much lower M_c of 0.0. This is supported by the detection of few $M_w < 0.0$ events outside of the hours of 1300–0500 (Ⓔ Fig. S12) because of higher daytime cultural noise. For this part of the catalog, we still cannot include the larger magnitudes with a single Gutenberg–Richter fit. We assume that this effect is due to M_c varying with time and our relatively small catalog of earthquakes undersampling the true earthquake sequence with a power-law distribution. In any case, we truncate the maximum magnitude at M_w 1.1. This yields a *b*-value of 1.2 (Fig. 7b), consistent with that of the larger events.

DISCUSSION

Based on the location of our interpreted subsurface faults and earthquake locations, we identify the causative fault for most of the earthquakes. Given this correlation, and computed moment tensors, the earthquakes most likely represent right-lateral strike-slip faulting along this west–east striking structure. In cross section, the double-difference relocations imply a steeply dipping fault plane (Fig. 6 and Ⓔ Fig. S6). At the earthquake source depths, according to interpreted well logs from HH-1 and Brockham, the rock types are mainly mudstone-rich Middle-Lower Jurassic to Upper Triassic sedimentary rocks. The stronger limestone unit of the Penarth formation at ∼2.3 km depth could promote the more brittle failure required for seismic slip.

There are few cases of very shallow (<3 km depth) natural earthquake sequences documented in the literature, but this is likely a result of suboptimal station coverage needed to accurately resolve such shallow depths. There are fewer documented cases of anomalously shallow natural earthquakes within sedimentary basins, with most past cases confined to metamorphic (Maceira *et al.*, 2000; Bent *et al.*, 2017) and igneous lithologies (Malone *et al.*, 1975). Many earthquakes in the United Kingdom with the most accurate depths lie between 5 and 15 km—that is, in the shallow to midcrust, although many events have shallower, and often poorly constrained depths. However, reanalysis of the 2005 Billingshurst sequence, 25–30 km to the south–west of Newdigate, suggested shallow event depths (Baptie and Luckett, 2018).

Most documented cases of shallow seismicity in stable continental regions worldwide link such seismicity with induced causes, in which dense seismic monitoring infrastructure were usually already in place. Such induced causes include hydraulic fracturing (Clarke *et al.*, 2014; Eaton *et al.*, 2018), conventional oil production (Willacy *et al.*, 2018), and groundwater extraction (González *et al.*, 2012).

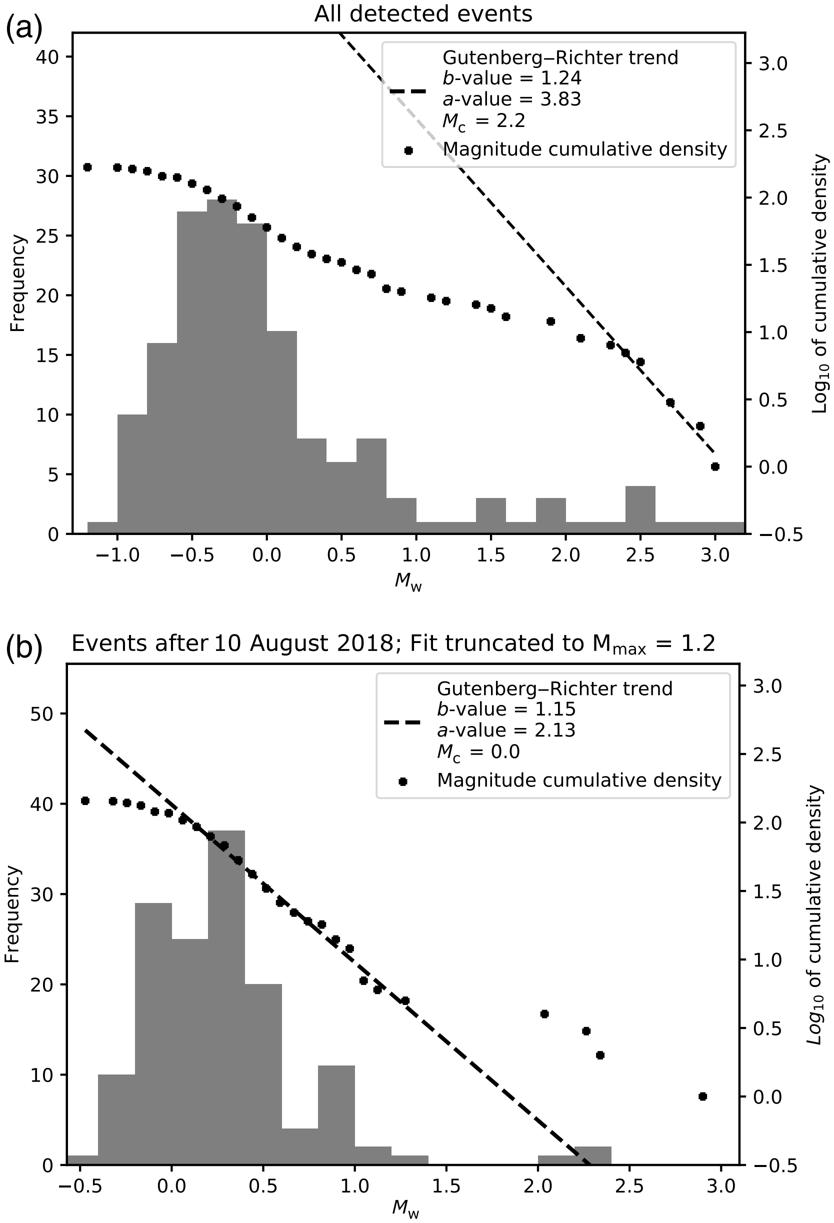

▲ **Figure 7.** Individual and cumulative frequency–magnitude distributions together with Gutenberg–Richter (G-R) relationship fits for (a) the entire sequence and (b) the sequence recorded by the temporary local monitoring network, with magnitudes scaled to an equivalent M_w, and G–R fits truncated to maximum magnitude of 1.2.

Given the location of the earthquakes, it is important to assess whether nearby oilfield activities induced these events or whether they were natural. As a first step, we first consider the problem within the framework of some of the key criteria established by Davis and Frohlich (1993) and Frohlich *et al.* (2016).

1. Past precedence: There are no known past earthquakes associated with oil and gas activities in southeast England, also an area of low seismicity (Fig. 1). The 2005 Billingshurst earthquakes in the Weald are the nearest analog to the Newdigate events as they occurred at a shallow depth (~5 km, yet poorly constrained) but not close to any known hydrocarbon activities. The long-term magnitude of completeness of the BGS seismicity catalog for the entire United Kingdom is approximately M_L 3.0 (Musson and Sargeant, 2007); therefore, we cannot rule out smaller past earthquakes in the area. Induced seismicity has been associated with hydraulic fracturing for shale gas in northern England (Clarke *et al.*, 2014) and conventional hydrocarbon extraction in the North Sea (Ottemöller *et al.*, 2005; Wilson *et al.*, 2015). Yet no documented cases exist of conventional onshore oil or gas extraction causing induced seismicity on the British Isles. Compared to the North Sea, onshore reservoirs in the United Kingdom typically produce hydrocarbons at much smaller volumes and rates.
2. Spatial correlation with industrial activities: Figure 1 shows that the Newdigate earthquake cluster occurred 3–5 km away from HH-1 and 6–8 km from the Brockham site. Seismicity caused by high-rate and high-volume fluid injection has been shown to induce earthquakes over long distances (>10 km) due to poroelastic stress transfer, particularly for high-volume injection into high-permeability sediments (Goebel *et al.*, 2017; Goebel and Brodsky, 2018). However, we do not believe that this triggering mechanism applies to the Surrey earthquakes given the comparatively very small injection operations (discussed further subsequently). We find no events at closer distances to HH-1; nor do we find any systematic migration of seismicity with time either away from or toward HH-1. The earthquakes are 1.0–1.5 km deeper than the Portland and Kimmeridge targets, which lie at ~600–700 and ~700–1000 m depth, respectively (Fig. 6). The earthquakes also likely occurred within either Triassic sedimentary rocks or the underlying deformed Palaeozoic rocks. Again, the linear group of epicenters appears to line up along the mapped NGF (Fig. 2).
3. Temporal links with industrial activities. Although oil license sites lie close to the seismic cluster, we also need to consider whether the earthquakes temporally correlate with oilfield activities. Figure 3 shows a timeline of seismicity and nearby well operations. After a two-year pause, production and associated injection activities resumed at the Brockham site in March 2018, two weeks before the first earthquake on 1 April 2018. Therefore, a coincidence exists between the start of the seismicity and the restart in

activities at Brockham. However, fluids have been produced at Brockham for 14 yr previously without inducing known seismicity. Nevertheless, induced seismicity has often been shown to lag by many years the start of production in conventional, large hydrocarbon reservoirs (Maury *et al.*, 1990). Work was carried out at HH-1 in March 2018 (Fig. 3), shortly before the first earthquake on 1 April. According to operator logs, this work involved only preparing the site at the surface, and no subsurface work in the borehole took place. Flow testing at HH-1 occurred in February–March 2016, a long time before any seismicity, and then from July 2018, after the onset of the earthquakes (Fig. 3), so we find no direct temporal correlation. Looking at events with magnitudes much greater than M_c, we find that 30%–50% of earthquakes in our catalog occurred within 72 hr of a reported well shut-in day at HH-1, whereas only 13%–30% of events occurred during a period of oil production (Fig. 3). However, robustly determining any such correlation is uncertain; it depends on the lower magnitude threshold chosen, and it is difficult to remove the effect of aftershocks occurring very soon after mainshocks. For hydraulic fracturing and wastewater injection, seismicity rates generally diminish during well shut-in periods (Horton, 2012; Schultz *et al.*, 2016). For simultaneous extraction and injection, models show that the highest pore pressure disturbance along basement faults may occur after shut-in (Chang and Segall, 2016). For gas extraction, well shut-ins lead to an overall decrease in earthquakes, although some critically stressed faults may rupture many years later (Zbinden *et al.*, 2017).

Using the Frohlich *et al.* (2016) criteria, uncertainty arises from testing the questions posed, as we could classify the Newdigate sequence as either possibly induced or probably induced. However, this approach is likely an oversimplification as it does not consider uncertainties in the arising answers, detailed source parameters, or knowledge of fluid pressure or pathways (Verdon *et al.*, 2019). We therefore assess the seismic source parameters as to whether they indicate an induced or natural cause for the events. We then examine in more detail whether the oilfield activities conducted at HH-1 and Brockham had the potential to induce earthquakes.

The faulting mechanisms (Figs. 2 and 5) are similar to the overall pattern in the British Isles, in which strike-slip faulting dominates (Fig. 1; Baptie, 2010). The Newdigate earthquake focal mechanisms are consistent with the regional stress field with the maximum horizontal stress oriented northwest–southeast. None of our moment tensor solutions show a large non-double-couple component (Fig. 5), as is sometimes observed for induced earthquakes (Sileny, 2009; Wang *et al.*, 2018), although such a discriminant is by no means definitive, because many cases of induced seismicity have double-couple source mechanisms. In cases where seismicity is induced by compaction in a conventional reservoir, we expect normal faulting at the edges of the reservoir, and reverse faulting within the overburden (Segall, 1989). Such mechanisms have been observed for compaction-induced events at large, depleting hydrocarbon fields (Maury *et al.*, 1990; Ottemöller *et al.*, 2005; Wees *et al.*, 2014; Dahm *et al.*, 2015; Willacy *et al.*, 2018). However, for the Newdigate events, the lack of such dip-slip components in the computed focal mechanisms shows that a compaction or subsidence mechanism did not cause the earthquakes. There are some cases of hydrocarbon extraction-induced events causing seismic slip that is roughly consistent with regional stress directions (e.g., Wetmiller, 1986); however, these cases still show dip-slip fault motions, unlike the Newdigate sequence. For fluid injection on the other hand, faulting mechanisms are usually consistent with the regional state-of-stress (e.g., Clarke *et al.*, 2014; McNamara *et al.*, 2015), and so this would not rule out an injection-induced cause. However, there has been no reported injection at HH-1 aside from <100 m^3 in 2016 and 4 m^3 in November 2018 for acid washing during flow testing. Injection at Brockham is of produced water, with the volume injected being smaller than the volume produced from the same formation (Fig. 3), resulting in net fluid withdrawal.

The mean stress drop of 3.2 MPa, given the uncertainty in corner frequency estimates, is consistent with a wide range of values computed for past earthquakes in Britain (Baptie *et al.*, 2005; Ottemöller *et al.*, 2009). We can attribute this stress drop to the low-shear strength of sedimentary rocks (Ottemöller *et al.*, 2005). Debate continues on whether we can use stress drop as an indicator of the events being induced. Hough (2014) suggests that induced earthquakes may have stress drops up to 10 times weaker than natural events of similar magnitudes based on ground-shaking intensity. However, Zhang *et al.* (2016) found no significant stress-drop variation between induced and natural earthquakes. Regardless, we find no evidence for an abnormally very high or very low stress drop for the Surrey events.

The Gutenberg–Richter *b*-value can give insights into the underlying causes of earthquakes. Seismicity caused by tectonic stresses on pre-existing faults usually has a *b*-value close to unity. Conversely, seismicity induced by fluid-related processes, whether natural (Wyss *et al.*, 1997) or because of fluid injection (Maxwell *et al.*, 2012), often has a higher *b*-value. The relatively small size of our catalog means that our computed *b*-value is poorly constrained, but our best estimates suggest it is close to the global average of 1.0. However, this does not on its own rule out a causal link with industrial activities, as many cases of induced seismicity produce *b*-values close to 1. But overall, this *b*-value suggests seismicity controlled by tectonic stresses along a pre-existing fault, consistent with the imaged fault structures (Figs. 2 and 6).

In summary, therefore, our observations of seismic source parameters are consistent with tectonic earthquakes. Given the regional stress tensor, uncertainties in the style of faulting and the static stress changes associated with the M_w >2 earthquakes in this sequence, it is likely that static stress triggering played a role (Ⓔ Fig. S10). We are not required to invoke fluid pressure changes, which have been used in other cases to explain the spatiotemporal evolution of injection-induced seismicity (Catalli *et al.*, 2013).

To our knowledge, seismicity caused by extraction has only been reported at very large hydrocarbon fields where production has taken place for many years. In contrast, the relatively small extraction volumes and rates at Brockham and HH-1 (Fig. 3) are unlikely to promote overburden failure. Compared to large oilfields globally, the Brockham reservoir is small, with only $\sim 60,000$ m^3 reported oil and water produced at low rates of extraction since 2002 (Fig. 3). This volume is several orders of magnitude smaller than reservoirs where well-documented production-induced seismicity occurred (e.g., Segall, 1989; Willacy *et al.*, 2018). At Brockham, production over roughly 15 yr has been balanced by reinjection of produced formation water back into the reservoir. Also, the injection of produced water into a depleted reservoir from which oil has been extracted is unlikely to increase the pressure in the reservoir to above preproduction levels, making induced seismicity less likely (Rubinstein and Mahani, 2015). Overall, more fluid has been extracted than withdrawn, so the net fluid balance is negative, and pore pressures in the Brockham field will be lower than when the reservoir was first produced from. Many east–west and east-northeast–west-southwest-striking faults between Brockham and the NGF (Figs. 2 and 6) likely act as a baffle to fluids or hydraulic pressure migrating toward the earthquake source region. As a result, injection at Brockham can be ruled out as a cause.

At HH-1, during the 2016 flow test, the operator injected approximately 50 m^3 acid and water to open fractures in the Kimmeridge at a rate of 0.24 m^3/min and a surface pressure of 10 MPa. A short period of oil flow then followed. Compared to well-studied cases of injection-induced seismicity in the United States (e.g., Frohlich, 2012), these volumes and rates at HH-1 are much smaller. Also, the flow testing that followed the acid injection would likely offset any transient pressure increase. With a gap of over two years between acid wash at HH-1 and the first earthquake, a mechanism involving a time lag of such duration is unlikely given the small volumes injected.

The earthquakes began in April 2018, predating the second phase of flow testing at HH-1 that began on 9 July 2018 (Fig. 3). The second major cluster of earthquakes had also occurred by this time. Based on available operational data, this eliminates HH-1 as a direct cause for these events.

The toe of the HH-1 well is close to the Horse Hill fault but does not appear to intersect it (Fig. 2), although we cannot estimate a fault damage zone width. However, the Portland and Kimmeridge Clay lie closer to the top-hole location of the well, and according to the operator, are isolated from the bottom of the well with three cement plugs. Hypothetically, a structural connection between the Horse Hill fault and NGF could support this triggering mechanism by acting as a conduit for fluid and pressure changes. Based on the available 2D seismic profiles, although we cannot completely rule out a diffuse fault transfer zone between the north-dipping Horse Hill fault and south-dipping NGF, we find no clear evidence to suggest that these faults intersect at depth.

The final possibility is that the first events of the seismic sequence were natural, but then flow testing work at HH-1 subsequently induced a resumption of seismicity. If so, the only causative mechanism would be one of extraction and pore pressure drawdown (Teufel *et al.*, 1991). Induced seismicity at conventional hydrocarbon fields is typically produced by compaction and slip within the overburden, which requires high-production volumes from large, laterally extensive fields. At HH-1, the volumes produced to date are small (~ 7000 m^3), and oil has only been produced for a very short time. We are not aware of any extraction-and-subsidence related seismicity for such small fluid volumes reported in the scientific literature. As discussed earlier, we would expect to see dip-slip motions associated with compaction, rather than the observed strike-slip mechanisms. In such cases, we expect seismicity to occur within and around the zone affected by pore pressure drawdown. For such volumes, this zone is currently unlikely to extend more than a few hundred meters from the well bore, as confirmed by radius of investigation values reported by the operator in 2018 (Fig. 2); not 3 km away laterally and over 1 km below the reservoir.

CONCLUSIONS

Based on the available evidence and consideration of possible triggering mechanisms, we conclude that at present, it is unlikely that anthropogenic activities induced the 2018–2019 Newdigate seismic sequence. We draw this conclusion from the following key observations of seismicity and hydrocarbon operations:

1. Timing of the start of seismic activity: Based on operators' logs, the earthquake sequence started before subsurface activity and flow testing or production at HH-1 in 2018.
2. Location: The earthquakes occur at least 3 km from the nearest oilfield operations, which would be an abnormally long distance for production-induced seismicity based on past reported cases. The earthquakes did not occur directly above, within, or on the immediate flanks of the extraction reservoir, as is typical for compaction-induced seismicity (Segall and Fitzgerald, 1998). We see no significant migration in the seismicity with time toward or away the oil reservoirs.
3. Temporal correlation with ongoing oilfield activities: Based on detailed operational logs provided by the operators, we find no clear link between seismicity rate and cumulative oil production or activities at either HH-1 or Brockham. Some earthquakes occurred during well shut-in periods at HH-1, however if this is a factor, the stress transfer mechanism is unclear.
4. Source mechanisms: Highly double-couple strike-slip focal mechanisms are consistent with the regional state of stress and background seismicity in the United Kingdom. We do not find dip-slip faulting mechanisms that are observed for cases of production-induced seismicity (Segall, 1989).

The frequency–magnitude character of the seismicity is not abnormal and shows a tectonic control on the earthquakes, consistent with reactivation of a pre-existing fault. The presence of multiple faults imaged using 2D seismic and double-difference relocations may help to explain the swarm-like nature of the seismic sequence.

5. Fluid volumes and stress: The reported cumulative volumes of net production are many orders of magnitude smaller than past reported cases of extraction-induced seismicity. Therefore, for such volumes, we do not expect large-scale poroelastic stress changes >10 MPa, which might be needed to induce seismicity (Segall, 1989). Aside from a small volume injected for acid wash at HH-1 in 2016, long before the first earthquake, and small volumes of fluid reinjection at Brockham that are exceeded by production volumes, the volumes and rates involved are very small. These amounts are dwarfed by other reported cases of fluid injection-induced seismicity over large distances (Goebel and Brodsky, 2018). Static stress modeling shows that earthquakes likely triggered each other by loading multiple fault strands rather than any external driver of fluid pore pressure changes.
6. Fluid pathways: There is no obvious connection between the Horse Hill and NGFs that could plausibly offer a permeability pathway from HH-1 to the earthquakes. Many west–east-trending normal faults likely act as a baffle to fluid flow to or from Brockham.

If all or some earthquakes were induced or triggered, then it would represent a novel mechanism not previously recognized for this style of oil extraction at the reported volumes. We have shown that seismic activity can occur at shallow depths in sedimentary basins, especially where pre-existing faults are optimally oriented for reactivation in the regional stress field. This result has implications for understanding the background rate of seismicity close to hydrocarbon exploration targets. Such shallow seismicity could pose a moderate seismic hazard to areas of high-population density. Based on 2D seismic profiles, for this area of southeast England, east–west-striking faults with a normal sense of offset, and likely optimally oriented in the regional stress field, are widespread. Moreover, operators and regulators could consider operating small seismic monitoring networks near conventional oilfield operations to better understand any nearby emergent seismic sequences earlier and to reduce uncertainties.

The 2018–2019 Newdigate seismic sequence was a contentious issue among members of the public, oilfield operators, and campaign groups. Without detailed seismic observations offered by the installed temporary seismic network and nearby citizen seismology sensors, large uncertainty over the causes of the sequence may have remained for the foreseeable future. Our knowledge of activities at Brockham and HH-1 relies on reported operational data provided by the operators. This source of data remains a controversial issue when determining induced versus natural causes of earthquakes. This particularly applies to industrial activities that lack any precedence for causing earthquakes, and for areas with a low rate of background seismicity. As operations continue in the long term, we recommend seismic monitoring close to hydrocarbon development and production sites, and high-resolution reporting of operational activities (e.g., well shut-in periods, production volumes, and rates) that is visible to the public. Over time, long-term monitoring could help reduce uncertainties in correlations and casual factors. We have shown that the 2018–2019 Newdigate, Surrey earthquakes offer new insight into the seismogenic potential of shallow sedimentary basins and the seismic hazard associated with these swarms.

DATA AND RESOURCES

All seismic waveform data and station metadata used in this study are available from the British Geological Survey (BGS, ftp://seiswav.bgs.ac.uk, last accessed May 2019) and from the RaspberryShake (RS) International Federation of Digital Seismograph Networks (FDSN) webservice (doi: 10.7914/SN/AM). All instrumentation for the temporary seismic stations were provided by the BGS. Operational data from Brockham and Horse Hill were provided by the operators of those fields, Angus Energy Plc., and UK Oil and Gas, respectively. We made figures using the Matplotlib (Hunter, 2007), Generic Mapping Tool (GMT, Wessel and Smith, 1998), and EQcorrscan (Chamberlain *et al.*, 2018) packages.

ACKNOWLEDGMENTS

The authors thank UK Oil and Gas Plc. and Angus Energy Plc. for providing operational data and sonic well logs. The authors are also grateful to the UK Oil and Gas Authority for organizing a workshop on the Newdigate earthquakes, which resulted in very fruitful scientific discussions with all participants. The authors also thank Branden Christensen and Angel Rodriguez, and their team at RaspberryShake (RS)/OSOP, S.A. for their co-operation when working with the community data. The authors are grateful for discussions with: Al Fraser on subsurface fault mapping, Antony Butcher on *b*-value determination, and Anthony Lomax for help with the NonLinLoc software. The authors thank Nicholas Booth, the owner of RS station AM.REC60 for continuing to maintain the monitoring effort throughout the Newdigate earthquake sequence. The authors thank David Hawthorn and his team at the British Geological Survey (BGS) for installing the temporary seismic stations. Finally, the authors thank local landowners of the Newdigate–Charlwood area for allowing seismic stations to be installed. The authors are grateful to Editor-in-Chief Zhigang Peng and two anonymous reviewers for providing constructive feedback on this article. The authors declare that there are no conflicts of interest.

REFERENCES

Andrews, I. (2014). *The Jurassic Shales of the Weald Basin: Geology and Shale Oil and Shale Gas Resource Estimation*, available at http://nora.nerc.ac.uk/id/eprint/512569/ (last accessed July 2019).

Anthony, R. E., A. T. Ringler, D. C. Wilson, and E. Wolin (2018). Do low-cost seismographs perform well enough for your network? An overview of laboratory tests and field observations of the OSOP Raspberry Shake 4D, *Seismol. Res. Lett.* **90,** no. 1, 219–228, doi: 10.1785/0220180251.

Assumpção, M. (1981). The NW Scotland earthquake swarm of 1974, *Geophys. J. Int.* **67,** no. 3, 577–586, doi: 10.1111/j.1365-246x.1981.tb06938.x.

Baptie, B. (2010). Seismogenesis and state of stress in the UK, *Tectonophysics* **482,** nos. 1/4, 150–159.

Baptie, B., and R. Luckett (2018). The Newdigate earthquake sequence, *2018 British Geological Survey Internal Rept*, available at http://www.earthquakes.bgs.ac.uk/research/NewdigateEarthquakesReport.pdf (last accessed July 2019).

Baptie, B., and L. Ottemoeller (2003). The Manchester earthquake swarm of October 2002, *EGS-AGU-EUG Joint Assembly*, Nice, France, 6 France–11 April 2003, available at http://adsabs.harvard.edu/abs/2003EAEJA....10286B (last accessed July 2019).

Baptie, B., L. Ottemöller, S. Sargeant, G. Ford, and A. O'Mongain (2005). The Dudley earthquake of 2002: A moderate sized earthquake in the UK, *Tectonophysics* **401,** nos. 1/2, 1–22.

Bent, A. L., S. Halchuk, V. Peci, K. E. Butler, K. B. Burke, J. Adams, N. Dahal, and S. Hayek (2017). The McAdam, New Brunswick, earthquake swarms of 2012 and 2015–2016: Extremely shallow, natural events, *Seismol. Res. Lett.* **88,** no. 6, 1586–1600, doi: 10.1785/0220170071.

Bishop, I., P. Styles, and M. Allen (1993). Mining-induced seismicity in the Nottinghamshire Coalfield, *Q. J. Eng. Geol. Hydrogeol.* **26,** no. 4, 253–279, doi: 10.1144/gsl.qjegh.1993.026.004.03.

British Geological Survey (BGS) (2010). *Detection Capability*, available at http://www.earthquakes.bgs.ac.uk/monitoring/detection_capability.html (last accessed July 2019).

British Geological Survey (BGS) (2019). Earthquakes near Newdigate, Surrey, British Geological Survey, available at http://earthquakes.bgs.ac.uk/research/SurreyEarthquakes.html (last accessed June 2019).

Brune, J. N. (1970). Tectonic stress and the spectra of seismic shear waves from earthquakes, *J. Geophys. Res.* **75,** 4997–5009, doi: 10.1029/JB075i026p04997.

Butler, M., and C. P. Pullan (1990). Tertiary structures and hydrocarbon entrapment in the Weald Basin of southern England, *Geol. Soc. Lond. Spec. Publ.* **55,** no. 1, 371–391, doi: 10.1144/gsl.sp.1990.055.01.19.

Catalli, F., M. Meier, and S. Wiemer (2013). The role of Coulomb stress changes for injection-induced seismicity: The Basel enhanced geothermal system, *Geophys. Res. Lett.* **40,** no. 1, 72–77, doi: 10.1029/2012gl054147.

Chamberlain, C. J., C. J. Hopp, C. M. Boese, E. Smith, D. Chambers, S. X. Chu, K. Michailos, and J. Townend (2018). EQcorrscan: Repeating and near-repeating earthquake detection and analysis in Python, *Seismol. Res. Lett.* **89,** no. 1, 173–181, doi: 10.1785/0220170151.

Chang, K., and P. Segall (2016). Seismicity on basement faults induced by simultaneous fluid injection-extraction, *Pure Appl. Geophys.* **173,** no. 8, 2621–2636, doi: 10.1007/s00024-016-1319-7.

Clarke, H., L. Eisner, P. Styles, and P. Turner (2014). Felt seismicity associated with shale gas hydraulic fracturing: The first documented example in Europe, *Geophys. Res. Lett.* **41,** no. 23, 8308–8314, doi: 10.1002/2014gl062047.

Clarke, H., J. P. Verdon, T. Kettlety, A. F. Baird, and J.-M. Kendall (2019). Real time imaging, forecasting and management of human-induced seismicity at Preston New Road, Lancashire, England, *Seismol. Res. Lett.* doi: 10.1785/0220190110.

Dahm, T., S. Cesca, S. Hainzl, T. Braun, and F. Krüger (2015). Discrimination between induced, triggered, and natural earthquakes close to hydrocarbon reservoirs: A probabilistic approach based on the modeling of depletion-induced stress changes and seismological source parameters, *J. Geophys. Res.* **120,** no. 4, 2491–2509, doi: 10.1002/2014jb011778.

Davis, S. D., and C. Frohlich (1993). Did (or will) fluid injection cause earthquakes?—Criteria for a rational assessment, *Seismol. Res. Lett.* **64,** nos. 3/4, 207–224.

Eaton, D. W., N. Igonin, A. Poulin, R. Weir, H. Zhang, S. Pellegrino, and G. Rodriguez (2018). Induced seismicity characterization during hydraulic-fracture monitoring with a shallow-wellbore geophone array and broadband sensors, *Seismol. Res. Lett.* **89,** no. 5, 1641–1651, doi: 10.1785/0220180055.

Frohlich, C. (2012). Two-year survey comparing earthquake activity and injection-well locations in the Barnett Shale, Texas, *Proc. Natl. Acad. Sci.* **109,** no. 35, 13,934–13,938, doi: 10.1073/pnas.1207728109.

Frohlich, C., H. DeShon, B. Stump, C. Hayward, M. Hornbach, and J. I. Walter (2016). A historical review of induced earthquakes in Texas, *Seismol. Res. Lett.* **87,** no. 4, 1022–1038, doi: 10.1785/0220160016.

García-Moreno, D., K. Verbeeck, T. Camelbeeck, M. De Batist, F. Oggioni, Z. O. Hurtado, W. Versteeg, H. Jomard, J. Collier, S. Gupta, *et al.* (2015). Fault activity in the epicentral area of the 1580 Dover Strait (Pas-de-Calais) earthquake (northwestern Europe), *Geophys. J. Int.* **201,** no. 2, 528–542, doi: 10.1093/gji/ggv041.

Goebel, T. H. W., and E. E. Brodsky (2018). The spatial footprint of injection wells in a global compilation of induced earthquake sequences, *Science* **361,** no. 6405, 899–904, doi: 10.1126/science.aat5449.

Goebel, T. H. W., M. Weingarten, X. Chen, J. Haffener, and E. E. Brodsky (2017). The 2016 Mw5.1 Fairview, Oklahoma earthquakes: Evidence for long-range poroelastic triggering at >40 km from fluid disposal wells, *Earth Planet. Sci. Lett.* **472,** 50–61, doi: 10.1016/j.epsl.2017.05.011.

González, P. J., K. F. Tiampo, M. Palano, F. Cannavó, and J. Fernández (2012). The 2011 Lorca earthquake slip distribution controlled by groundwater crustal unloading, *Nature Geosci.* **5,** no. 11, 821–825, doi: 10.1038/ngeo1610.

Grigoli, F., S. Cesca, E. Priolo, A. Rinaldi, J. F. Clinton, T. A. Stabile, B. Dost, M. Fernandez, S. Wiemer, and T. Dahm (2017). Current challenges in monitoring, discrimination, and management of induced seismicity related to underground industrial activities: A European perspective, *Rev. Geophys.* **55,** no. 2, 310–340, doi: 10.1002/2016RG000542.

Grünthal, G. (1998). *European Macroseismic Scale 1998 EMS-98*, Cahiers du Centre Européen de Géodynamique et de Seismologie, Conseil de l'Europe, Luxembourg, Europe.

Hansen, D. L., D. J. Blundell, and S. B. Nielsen (2002). A model for the evolution of the Weald Basin, *Bull. Geol. Soc. Denmark* **49,** 109–118.

Häring, M. O., U. Schanz, F. Ladner, and B. C. Dyer (2008). Characterisation of the Basel 1 enhanced geothermal system, *Geothermics* **37,** no. 5, 469–495, doi: 10.1016/j.geothermics.2008.06.002.

Heimann, S. (2016). Sebastian Heimann/lassie, *GitLab*, available at https://gitext.gfz-potsdam.de/heimann/lassie (last accessed June 2019).

Horton, S. (2012). Disposal of hydrofracking waste fluid by injection into subsurface aquifers triggers earthquake swarm in Central Arkansas with potential for damaging earthquake, *Seismol. Res. Lett.* **83,** no. 2, 250–260, doi: 10.1785/gssrl.83.2.250.

Hough, S. (2014). Shaking from injection-induced earthquakes in the Central and Eastern United States, *Bull. Seismol. Soc. Am.* **104,** no. 5, 2619–2626, doi: 10.1785/0120140099.

Hunter, J. D. (2007). Matplotlib: A 2D graphics environment, *Comput. Sci. Eng.* **9,** no. 3, 90–95.

Kaven, J., S. Hickman, A. McGarr, and W. Ellsworth (2015). Surface monitoring of microseismicity at the Decatur, Illinois, CO_2 sequestration demonstration site, *Seismol. Res. Lett.* **86,** no. 4, 1096–1101, doi: 10.1785/0220150062.

Keranen, K., M. Weingarten, G. Abers, B. A. Bekins, and S. Ge (2014). Sharp increase in central Oklahoma seismicity since 2008 induced by massive wastewater injection, *Science* **345,** no. 6195, 448–451, doi: 10.1126/science.1255802.

Kusznir, N., D. Ashwin, and A. Bradley (1980). Mining induced seismicity in the North Staffordshire coalfield, England, *Int. J. Rock Mech. Min. Sci. Geomech. Abstr.* **17,** no. 1, 45–55.

Lomax, A., A. Michelini, and A. Curtis (2009). Earthquake location, direct, global-search methods, in *Encyclopedia of Complexity and Systems Science*, R. A. Myers (Editor), Springer, New York, New York, 2449–2473, doi: 10.1007/978-0-387-30440-3_150.

López-Comino, J. A., S. Cesca, J. Jarosławski, N. Montcoudiol, S. Heimann, T. Dahm, S. Lasocki, A. Gunning, P. Capuano, and W. L. Ellsworth (2018). Induced seismicity response of hydraulic fracturing: Results of a multidisciplinary monitoring at the Wysin site, Poland, *Sci. Rep.* **8,** no. 1, 8653, doi: 10.1038/s41598-018-26970-9.

Luckett, R., L. Ottemöller, A. Butcher, and B. Baptie (2019). Extending local magnitude ML to short distances, *Geophys. J. Int.* **216,** no. 2, 1145–1156, doi: 10.1093/gji/ggy484.

Maceira, M., C. J. Ammon, and R. Herrmann (2000). Faulting parameters of the September 25, 1998 Pymatuning, Pennsylvania earthquake, *Seismol. Res. Lett.* **71,** no. 6, 742–752, doi: 10.1785/gssrl.71.6.742.

Malone, S. D., G. H. Rothe, and S. W. Smith (1975). Details of microearthquake swarms in the Columbia Basin, Washington, *Bull. Seismol. Soc. Am.* **65,** no. 4, 855–864.

Maury, V., J. Grasso, and G. Wittlinger (1990). Lacq gas field (France): Monitoring of induced subsidence and seismicity consequences on gas production and field operation, *European Petroleum Conference*, The Hague, The Netherlands, 21–24 October, doi: 10.2118/20887-ms.

Maxwell, S., M. Jones, R. Parker, S. Miong, S. Leaney, D. Dorval, D. D'Amico, J. Logel, E. Anderson, and K. Hammermaster (2012). Fault activation during hydraulic fracturing, *SEG Technical Program Expanded Abstracts 2009*, Vol. 43, 1552–1556, doi: 10.1190/1.3255145.

McNamara, D., H. Benz, R. Herrmann, E. Bergman, P. Earle, A. Holland, R. Baldwin, and A. Gassner (2015). Earthquake hypocenters and focal mechanisms in central Oklahoma reveal a complex system of reactivated subsurface strike-slip faulting, *Geophys. Res. Lett.* **42,** no. 8, 2742–2749, doi: 10.1002/2014gl062730.

Musson, R. M. W. (1993). Comrie: A historical Scottish earthquake swarm and its place in the history of seismology, *Terra Nova* **5,** no. 5, 477–480, doi: 10.1111/j.1365-3121.1993.tb00288.x.

Musson, R. M. W. (1994). A catalogue of British earthquakes, *British Geol. Surv. Global Seismol. Rept. WL/94/04*.

Musson, R. M. W. (2008). The seismicity of the British Isles to 1600, *British Geol. Surv. Open Rept. OR/08/049*, available at `http://www.earthquakes.bgs.ac.uk/historical/data/studies/MUSS008/MUSS008.pdf` (last accessed July 2019).

Musson, R. M. W., and S. Sargeant (2007). Eurocode 8 seismic hazard zoning maps for the UK, *British Geol. Surv. Rept. CR/07/125*, available `http://nora.nerc.ac.uk/id/eprint/508595/` (last accessed July 2019).

Ogata, Y. (2005). Detection of anomalous seismicity as a stress change sensor, *J. Geophys. Res.* **110,** no. 5, 1–14, doi: 10.1029/2004JB003245.

Ottemöller, L., and C. Thomas (2007). Highland boundary fault zone: Tectonic implications of the Aberfoyle earthquake sequence of 2003, *Tectonophysics* **430,** nos. 1/4, 83–95.

Ottemöller, L., B. Baptie, and N. Smith (2009). Source parameters for the 28 April 2007 Mw 4.0 earthquake in Folkestone, United Kingdom, *Bull. Seismol. Soc. Am.* **99,** no. 3, 1853–1867, doi: 10.1785/0120080244.

Ottemöller, L., H. Nielsen, K. Atakan, J. Braunmiller, and J. Havskov (2005). The 7 May 2001 induced seismic event in the Ekofisk oil field, North Sea, *J. Geophys. Res.* **110,** no. B10, 379, doi: 10.1029/2004jb003374.

Pine, R., and A. Batchelor (2001). Downward migration of shearing in jointed rock during hydraulic injections, *Int. J. Rock Mech. Min. Sci. Geomech. Abstr.* **21,** no. 5, 249–263.

Redmayne, D. (1988). Mining induced seismicity in UK coalfields identified on the BGS National Seismograph Network, *Geol. Soc. Lond. Eng. Geol. Spec. Publ.* **5,** no. 1, 405–413, doi: 10.1144/gsl.eng.1988.005.01.45.

Rubinstein, J. L., and A. Mahani (2015). Myths and facts on wastewater injection, hydraulic fracturing, enhanced oil recovery, and induced seismicity, *Seismol. Res. Lett.* **86,** no. 4, 1060–1067, doi: 10.1785/0220150067.

Schultz, R., R. Wang, Y. Gu, K. Haug, and G. Atkinson (2016). A seismological overview of the induced earthquakes in the Duvernay play near Fox Creek, Alberta, *J. Geophys. Res.* **122,** 492–505, doi: 10.1002/2016JB013570.

Segall, P. (1989). Earthquakes triggered by fluid extraction, *Geology* **17,** no. 10, 942, doi: 10.1130/0091-7613(1989)017<0942:etbfe>2.3.co;2.

Segall, P., and S. D. Fitzgerald (1998). A note on induced stress changes in hydrocarbon and geothermal reservoirs, *Tectonophysics* **289,** nos. 1/3, 117–128, doi: 10.1016/s0040-1951(97)00311-9.

Sileny, J. (2009). Resolution of non-double-couple mechanisms: Simulation of hypocenter mislocation and velocity structure mismodeling, *Bull. Seismol. Soc. Am.* **99,** no. 4, 2265–2272, doi: 10.1785/0120080335.

Staudenmaier, N., T. Tormann, B. Edwards, N. Deichmann, and S. Wiemer (2018). Bilinearity in the Gutenberg–Richter relation based on M_L for magnitudes above and below 2, from systematic magnitude assessments in Parkfield (California), *Geophys. Res. Lett.* **45,** no. 14, 6887–6897, doi: 10.1029/2018gl078316.

Steacy, S., D. Marsan, S. S. Nalbant, and J. McCloskey (2004). Sensitivity of static stress calculations to the earthquake slip distribution, *J. Geophys. Res.* **109,** no. B4, doi: 10.1029/2002jb002365.

Teufel, L. W., D. W. Rhett, and H. E. Farrell (1991). Effect of reservoir depletion and pore pressure drawdown on in situ stress and deformation in the Ekofisk field, North Sea, *The 32nd US Symposium on Rock Mechanics (USRMS)*, Norman, Oklahoma, 10–12 July.

UK Onshore Geophysical Library (UKOGL) (2019). *UK Onshore Geophysical Library*, available at `https://ukogl.org.uk` (last accessed July 2019).

Verdon, J. P. (2014). Significance for secure CO2 storage of earthquakes induced by fluid injection, *Environ. Res. Lett.* **9,** no. 6, 064022, doi: 10.1088/1748-9326/9/6/064022.

Verdon, J. P., B. J. Baptie, and J. J. Bommer (2019). An improved framework for discriminating seismicity induced by industrial activities from natural earthquakes, *Seismol. Res. Lett.* **90,** no. 4, 1592–1611, doi: 10.1785/0220190030.

Verdon, J. P., J.-M. Kendall, A. Butcher, R. Luckett, and B. J. Baptie (2018). Seismicity induced by longwall coal mining at the Thoresby Colliery, Nottinghamshire, U.K., *Geophys. J. Int.* **212,** no. 2, 942–954, doi: 10.1093/gji/ggx465.

Waldhauser, F., and W. L. Ellsworth (2000). A double-difference earthquake location algorithm: Method and application to the northern Hayward Fault, California, *Bull. Seismol. Soc. Am.* **90,** no. 6, 1353–1368, doi: 10.1785/0120000006.

Wang, R., Y. Gu, R. Schultz, and Y. Chen (2018). Faults and non-double-couple components for induced earthquakes, *Geophys. Res. Lett.* **45,** no. 17, 8966–8975, doi: 10.1029/2018gl079027.

Webster, B. (2018). Hunt on for source of Surrey tremors, *The Times*, London, United Kingdom.

Wees, V. J., L. Buijze, K. van Thienen-Visser, M. Nepveu, B. Wassing, B. Orlic, and P. Fokker (2014). Geomechanics response and induced seismicity during gas field depletion in the Netherlands, *Geothermics* **52,** 206–219, doi: 10.1016/j.geothermics.2014.05.004.

Wessel, P., and R. Smith (1998). New, improved version of generic mapping tools released, *Eos Trans. AGU* **79,** no. 47, 579–579.

Wetmiller, R. J. (1986). Earthquakes near Rocky Mountain House, Alberta, and their relationship to gas production facilities, *Can. J. Earth Sci.* **23,** 172–181, doi: 10.1139/e86-020.

Wiemer, S., and M. Wyss (2000). Minimum magnitude of completeness in earthquake catalogs: Examples from Alaska, the Western United States, and Japan, *Bull. Seismol. Soc. Am.* **90,** no. 4, 859–869, doi: 10.1785/0119990114.

Willacy, C., E. van Dedem, S. Minisini, J. Li, J. Blokland, I. Das, and A. Droujinine (2018). Application of full-waveform event location and moment-tensor inversion for Groningen induced seismicity, *The Leading Edge* **37,** no. 2, 92–99, doi: 10.1190/tle37020092.1.

Wilson, M. P., R. J. Davies, G. R. Foulger, B. R. Julian, P. Styles, J. G. Gluyas, and S. Almond (2015). Anthropogenic earthquakes in the

UK: A national baseline prior to shale exploitation, *Mar. Petrol. Geol.* **68,** 1–17, doi: 10.1016/j.marpetgeo.2015.08.023.

Wyss, M., K. Shimazaki, and S. Wiemer (1997). Mapping active magma chambers by *b* values beneath the off-Ito volcano, Japan, *J. Geophys. Res.* **102,** no. B9, 20,413–20,422, doi: 10.1029/97jb01074.

Zbinden, D., A. Rinaldi, L. Urpi, and S. Wiemer (2017). On the physics-based processes behind production-induced seismicity in natural gas fields, *J. Geophys. Res.* **122,** no. 5, 3792–3812, doi: 10.1002/2017jb014003.

Zhang, H., D. W. Eaton, G. Li, Y. Liu, and R. M. Harrington (2016). Discriminating induced seismicity from natural earthquakes using moment tensors and source spectra, *J. Geophys. Res.* **121,** no. 2, 972–993, doi: 10.1002/2015jb012603.

Ziv, A., and A. M. Rubin (2000). Static stress transfer and earthquake triggering: No lower threshold in sight?, *J. Geophys. Res.* **105,** no. B6, 13,631–13,642.

Stephen P. Hicks
Department of Earth Science and Engineering
Imperial College London
Prince Consort Road, South Kensington
London SW7 2BP, United Kingdom
s.hicks@imperial.ac.uk

James Verdon
School of Earth Sciences
University of Bristol
Wills Memorial Building, Queens Road
Bristol BS8 1RL, United Kingdom

Brian Baptie
Richard Luckett
British Geological Survey, The Lyell Centre
Research Avenue South
Edinburgh EH14 4AP, United Kingdom

Zoë K. Mildon
School of Geography, Earth and Environmental Sciences
University of Plymouth
Drake Circus
Plymouth PL4 8AA, United Kingdom

Thomas Gernon
School of Ocean and Earth Science
University of Southampton, Waterfront Campus
National Oceanography Centre European Way
Southampton SO14 3ZH, United Kingdom